RESULTS OF 1 MeV PROTON IRRADIATION OF FRONT AND BACK SURFACES OF SILICON SOLAR CELLS

B.E. Anspaugh and R. Kachare
Jet Propulsion Laboratory
Pasadena, California

V.G. Weizer
NASA Lewis Research Center
Cleveland, Ohio

Several silicon solar cells with and without back surface fields (BSF), having thicknesses of 200 μm and 63 μm were irradiated with 1 MeV protons having fluences between 1 x 10^{10} and 1 x 10^{12} p/cm^2. The irradiation was performed using both normal and isotropic incidence on the front as well as back surfaces of the solar cells. The results of the back surface irradiations are analyzed by using a model in which irradiation-induced defects across the high-low (BSF) junction are considered. It is concluded that degradation of the high-low junction is responsible for the severe performance loss in thinner cells when irradiated from the rear.

INTRODUCTION

For the past several years most solar cell manufacturers have incorporated a back surface field in their solar cells in order to boost power output. The BSF has been particularly important in thin solar cells where the minority carrier diffusion length may be much larger than the thickness. Significant increases in power (as much as 28% for 63 μm thick cells) are achieved when the field is incorporated. However, BSF cells lose their output at a greater rate than their non-field counterparts when exposed to ionizing radiation typical of space exposures (ref. 1). The degradation of BSF cells with radiation has not been adequately modeled, and it is the purpose of this paper to explore the cell degradation with one specific energy of protons and compare the results with the predictions of a recent model describing the behavior of cells with defective BSFs (ref. 2).

EXPERIMENTAL PROCEDURE

The solar cells tested were made from 10 ohm-cm silicon. They all had dual antireflection coatings and aluminum back surface reflectors (BSR). Two thicknesses of solar cells were used, 63 μm and 200 μm. Half the cells of each thickness had back surface fields applied using aluminum paste, and half had no BSF. The cell manufacturer estimated that the junction depths were 0.25 μm, the BSFs penetrated into the cell ~ 5 μm and the thicknesses of the aluminum BSRs were 0.2 μm. All cells measured 2 x 2 cm.

The 1 MeV proton irradiations were performed at the Caltech 1 MeV van de Graaff accelerator facility using the techniques described in reference 3. The protons were spread out into a uniform beam at the target plane by use of a gold scattering foil about 2 μm thick. Two groups of cells were irradiated during each run, one group under front normal incidence, and the other group under simulated front isotropic incidence using the omnidirectional fixture (ref. 3). After the two groups of cells were irradiated in this manner, the irradiation was repeated with another two groups of cells with the protons incident on the rear cell surfaces. Light I-V curves before and after irradiation were taken with an X25 Solar Simulator simulating the air mass zero solar spectrum. This procedure was repeated 7 times with the same solar cells, increasing the fluence level each time until a total fluence of 1×10^{12} p/cm^2 had been accumulated. The cells were not annealed after irradiation, and in most cases were measured within an hour of the irradiation.

RESULTS AND DISCUSSION

Protons having an energy of 1 MeV will penetrate to different depths in silicon solar cells, depending on whether they are incident on the front or rear surfaces. They will go into the silicon 16.5 μm (ref. 4) when incident on the front, but due to the presence of the rear metal contact, they will only go into the silicon ~ 4 μm when incident on the rear. When protons are incident normally, they produce most of the displacement damage very near the end of their track, essentially producing a recombination zone which inhibits passage by minority carriers. But when protons are incident isotropically, they produce a rather smeared out damage profile which will be easier for minority carriers to cross. The use of 1 MeV protons was made in this investigation to selectively examine the effect of irradiation on the front portion of the cells where the junction is involved, and on the rear portion of the cells where the back surface field is involved.

Tables I and II show the values of I_{sc}, V_{oc}, P_{max}, and FF of 200 μm and 63 μm silicon solar cells respectively before and after 1 MeV proton irradiation to fluences of 1×10^{12} p/cm^2. The pre-irradiation data shows the advantage of using the BSF structures. For example, the fields increased cell performance in the 200 μm cells by ~ 20 mA in I_{sc}, 69 mV in V_{oc}, and 17 mW in P_{max} while in the 63 μm cells, the fields gave corresponding increases of ~ 15 mA, 90 mV, and 16 mW.

The advantage of the field is given up after front surface irradiations, however. As shown in the Tables, the electrical parameters of the 63 μm cells are essentially the same after either normal or omni irradiation, regardless of whether the cells began life with a BSF. In contrast, the thicker 200 μm cells with BSF retain slightly higher outputs cells after the 1 MeV front irradiations. This behavior is also depicted in figures 1 and 2 where P_{max} is plotted as a function of 1 MeV proton fluence. The data is illustrating that as the proton fluence is increased, the effectiveness of the BSF is reduced and nearly the same values of P_{max} should be observed irrespective of BSF and cell thickness.

A comparison of the differences between front surface omni vs. normal incidence irradiation reveals some interesting differences. For both cell thicknesses, the omni irradiation is not as damaging for either I_{sc} or P_{max}. But for V_{oc}, the end result after $\Phi = 1 \times 10^{12}$ p/cm^2 is exactly the same.

When the non-BSF cells of either thickness are irradiated from the rear with omnidirectional protons, there is almost no degradation of the solar cell parameters. This is not true of the BSF cells, however. The 63 μm BSF cells with fields degrade more than the non-BSF cells under these conditions. The opposite

is true of the 200 μm BSF cells where the BSF cells retain higher outputs after the rear omni irradiations.

Examining the case for rear normal irradiation, we find degradation in all cell types. Here too, the 63 μm cells with fields degrade more than their non-BSF counterparts. The 200 μm cells with fields degrade at a faster rate than their non-field counterparts, but they retain more absolute power. Figures 3 through 5 illustrate the degradation of the various cell parameters under normal rear incidence irradiation. Figure 3 illustrates that negligibly small changes occurred in the I_{sc} values of non-BSF cells of either thickness. However, significantly large degradations in I_{sc} values are seen in both thicknesses of BSF cells. The 63 μm BSF cells retain their I_{sc} advantage over the non-BSF cells until fluences greater than 1×10^{11} p/cm^2 are reached, but from then on, the non-BSF cells were superior. This behavior, which has been observed a sufficient number of times to establish statistical validity, is not understood. The I_{sc} values for 200 μm BSF cells also degrade under this irradiation geometry, but they retain their advantage over the non-BSF cells over the entire fluence range. The I_{sc} degradation curves for both thicknesses of BSF cells appear to exhibit a plateau effect such that after reaching a certain fluence, no further degradation will occur. For 200 μm cells, this plateau occurs at $\sim 3 \times 10^{11}$ p/cm^2 and for the 63 μm cells, the plateau is not fully developed, but appears to occur at slightly higher fluences.

The variation of V_{oc} as a function of 1 MeV protons normally incident on the rear cell surfaces is presented in figure 4. Negligibly small changes in V_{oc} for non-BSF cells were observed. However, dramatic reductions in the V_{oc} values with increasing fluence in 63 μm BSF cells were noted and V_{oc} was reduced to less than the corresponding V_{oc} values of non-BSF cells after $\Phi > 2 \times 10^{11}$ p/cm^2.

Figure 5 gives the change in P_{max} as a function of 1 MeV proton fluence incident normally on the rear surfaces. As for I_{sc} and V_{oc}, the non-BSF cells do not degrade with fluence, but here that is only true for fluences less than 1×10^{11} p/cm^2, after which they begin degradation. The P_{max} degradation for 63 μm BSF cells occurs at a more rapid rate than for any other cell type, and these cells lose their power advantage over the 63 μm non-BSF cells after $\Phi > 2 \times 10^{11}$ p/cm^2.

Figure 6 depicts the variation of P_{max} as a function of fluence of 1 MeV protons with omnidirectional incidence on the rear surfaces. Here there is no P_{max} degradation of cells without BSF, nor do the BSF cells degrade as severely as observed for the rear normal incidence cases shown in figure 5. Also, the BSF effect in 63 μm cells is preserved up through $\Phi = 5 \times 10^{11}$ p/cm^2.

The important point to be made here is that though significant improvement in 63 μm cell performance is achieved by using a BSF, it is totally reduced to less than the non-BSF cell performance level after high fluences of low energy protons. Fields in the thicker cells do not enhance the cell performance quite as markedly as they do for thinner cells, but the thicker cells retain some of their advantage after irradiation to these same levels.

MODEL CALCULATIONS

Front Surface Irradiations

Since the projected range of 1 MeV front surface normally incident protons is 16.5 μm, we attempted to analyze the data by dividing the cell into two regions, one inner irradiated region (16 μm thick) and the other consisting of a deeper non-damaged region (184 μm thick). As a first approximation, we assumed that in the damaged region only the minority carrier lifetime is uniformly degraded throughout the 16 μm layer. We also assumed that with a proton fluence of 1×10^{12} p/cm^2, heavy damage has been introduced at the end of the proton track and consequently

for front surface irradiations, the BSF and non-BSF cells are similar. This rationale appears to be acceptable based on the results shown in figures 1 and 2.

The experimental I_{sc} and V_{oc} values before irradiation were fitted to the standard solar cell equations (ref. 5) using suitable values for 10 ohm-cm silicon, e.g. the diffusion constant D = 30 cm^2/sec, the dopant concentration, N_A = 1.3 x 10^{15} cm^{-3}, and back surface recombination velocities, S_B values of 10 cm/sec and 10^8 cm/sec, for BSF and non-BSF cells respectively. Minority carrier diffusion length (L_n) values of 600 μm were found to fit the pre-irradiation data for both BSF and non-BSF cells.

Various calculations were made to fit the post-irradiation I_{sc} and V_{oc} values. In these calculations, only L_n values for the inner layer were varied in order to fit the data. The calculated I_{sc} and V_{oc} values were significantly affected only when L_n values for the inner layers were made less than 16 μm. For both BSF and non-BSF cells under normal incidence, L_n values of 4 μm for the inner layer gave good fits to the data, and L_n values of about 6 μm gave good fits to the omnidirectional data.

It should be pointed out that if values of D, L_n, S_B, and intrinsic carrier concentration (n_i), are varied, then several sets of these parameters could conceivably give fits to the experimental data. This problem in the calculation can be reduced by subdividing the damaged layer into multi-layers (refs. 6 and 7) which take into account the non-uniformity of proton irradiation, and assigning appropriate parameters to each layer. However, such calculations are highly complicated and are not considered here.

Back Surface Irradiations

Figures 3 through 6 show that rear surface normal and omnidirectional protons do not degrade non-BSF cells except for fluences greater than 1 x 10^{10} p/cm^2 at normal incidence. As can be seen in Tables I and II, the fill factors (FF) of these cells are significantly reduced after normal incidence irradiation of 10^{12} p/cm^2. This change in FF could be due to an increase in dark saturation current in the base, I_{ob}, an increase in series resistance, R_s, or a decrease in the shunt resistance, R_{sh}. Changes in R_{sh} and I_{ob} will have a major effect on the degradation of V_{oc} and an increase in R_s will degrade I_{sc} (ref. 5). Since significant reductions in V_{oc} are observed compared to those in I_{sc}, it would appear that major changes in R_{sh} and I_{ob} are occurring. Also some increase in R_s may be expected with such a high fluence due to majority carrier removal (ref. 8). I_{ob} will increase due to decreases in L_n and D due to radiation-induced defects. Since the non-BSF cells are not degraded as badly as the BSF cells, we will focus our attention on the degradation in the BSF cells.

Since the 1 MeV protons are stopping in the pp+ region, they will produce maximum damage to the high-low junction. The energy levels and density of these defects depend strongly on the fluence and irradiation configuration. Omni-directional incidence protons will induce defects that are spatially smeared in the entire BSF region whereas normal incidence protons will produce highly localized large defect concentrations in the vicinity of the pp+ junction. Consequently, a more defective BSF is produced by the normal incidence protons than by the omni protons. This is reflected in the experimental data of figures 3 through 6.

Attempts were made to explain the degradation of BSF cells using the existing models (refs. 2 and 9). In the Sah model (ref. 9) the effects of defects distributed in the bulk across the BSF are analyzed by using three regions in a defective unit cell containing one defect. The width of the first region surrounding the defect is characterized by the distance-of-influence which is about two diffusion lengths. The defect itself is characterized by three parameters, namely, defect density, defect area and the surface recombination velocity at the

defective area. The model predicts very substantial degradation of V_{oc} even if there are only 40 defects/cm^2 (ref. 9). If this would have been the case, then the V_{oc} values shown in figure 4 and the P_{max} values shown in figures 5 and 6 would have been rapidly degraded with fluences less than 1 x 10^{11} p/cm^2. Since this is not so, this model apparently over-estimates the cell degradation (ref. 2).

The other model is described in detail in reference 2. The important finding of this model analysis is that it is possible to have a fully effective BSF region, regardless of the spatial distribution of the defective areas as long as the total defective area is reduced below certain limits. A case of distributed defects discussed in reference 2 closely matches the defect geometry induced in the BSF region by low energy protons. Modifying eq. 8 (ref. 2) for the distributed defect case to match the degradation in V_{oc} by low energy protons in BSF cells, we obtain:

$$dV_{oc} = KT \ln \left[\frac{J_{sc1} \left(S' + \tanh d/L_n \right)}{J_{sc2} \left(\tanh d/L_n + S' \tanh^2 d/L_n \right)} \right] \qquad (1)$$

where J_{sc1} and J_{sc2} are the short circuit currents of the BSF cells before and after irradiation respectively and

$$S' = 5 \times 10^6 \left[\frac{f}{2 - f} \right] \frac{L_n}{D_n} \qquad (2)$$

where S' is a normalized rear surface recombination velocity, S_B, f is the fraction of the BSF area which is defective, and d is the cell thickness.

The change in S' as a function of Φ can be calculated using equation (1) and the corresponding value of f can then be obtained from equation (2). S_B is given by (ref. 2):

$$S_B = \frac{V}{2} \left[\frac{f}{2 - f} \right] \qquad (3)$$

where V is the carrier thermal velocity which for silicon is ~ 10^7 cm/sec.

Several runs were made using various values of L_n while holding D constant at 30 cm^2/sec. Figure 7 illustrates the results of our model calculation where the back surface recombination velocity plots as a function of proton fluence are given for 200 μm and 63 μm BSF cells having L_n = 800 and 600 μm respectively. As can be seen, S_B increases with Φ, and it increases at a different rate for normal incidence than it does for omnidirectional incidence. These results clearly demonstrate that as the BSF becomes defective, S_B tends to increase. Thus the cell performance which has been improved by using a BSF has been mostly degraded after irradiation. In general, for a given fluence there is more increase in S_B for rear normal incidence than that for omnidirectional irradiation. S_B values of 5.36 x 10^5 cm/sec and 1.07 x 10^4 cm/sec were calculated for 200 μm and 63 μm BSF cells respectively after rear normal irradiation with Φ = 1 x 10^{12} p/cm^2.

It is gratifying to find that such a simple model can provide quantitative changes in the trend of S_B as a function of fluence. However, to obtain an in-depth understanding of damage mechanism of the BSF, the model would probably have to be refined to take into account the leakage in the high-low junction, changes in the recombination velocity at the pp+ junction, and the change in L_n in the p+ region with fluence. In addition it may be necessary to consider imperfections in the Al paste alloying, impurities in the paste, and an imperfect Al profile.

CONCLUSIONS

Of the four radiation geometries observed, the front surface normal incidence irradiation was the most effective in producing degradation in both thick and thin cells with and without BSF.

No significant cell degradation was observed in either thick or thin non-BSF cells when irradiated from the rear surface with 1 MeV protons.

After rear surface normal and omnidirectional irradiation with fluences of 1 x 10^{12} p/cm^2, all the BSF cells degrade at a faster rate than cells without BSF. However, the 200 μm BSF cells retain more absolute power than comparable non-BSF cells, but 63 μm BSF cells retain less absolute power than comparable non-BSF cells.

A simple model was used to calculate the back surface recombination velocity and explain the rear incidence proton irradiation damage in both thick and thin BSF cells.

Additional rear surface irradiation experiments with the cells having BSF made by boron diffusion, ion implantation and Al diffusion coupled with a refined model which will take into account high-low junction related device parameters will be required to fully understand the defective BSF and its role, particularly in thin cells.

REFERENCES

1. H. Y. Tada, Jr. R. Carter, Jr., B. E. Anspaugh, and R. G. Downing, Solar Cell Radiation Handbook, JPL Publication 82-69, Jet Propulsion Laboratory, Pasadena, California, Nov. 1982.
2. V. G. Weizer, "The Effect of a Defective BSF Layer on Solar Cell Open Circuit Voltage," Solar Cells, 14, 1985, p. 241.
3. B. E. Anspaugh and R. G. Downing, "Radiation Effects in Silicon and Gallium Arsenide Solar Cells Using Isotropic and Normally Incident Radiation," JPL Publication 84-61, Jet Propulsion Laboratory, Pasadena, California, Sept., 1984.
4. J. F. Janni, "Proton Range-Energy Tables, 1 keV-10GeV," Atomic Data and Nuclear Data Tables, 27, Nos. 4/5, July/Sept., 1982.
5. H. J. Hovel, Semiconductors and Semimetals, Vol. 11, Solar Cells, Academic Press, New York, 1975.
6. I. Nashiyama, E. Teranishi, and M. Kageyama, "Protons and Deuteron Irradiation Damage in Silicon Solar Cells," Jap. Jour. of Appl. Physics, 10, No. 11, Nov., 1971, p. 1564.
7. D. L. Crowther, E. A. Loda, J. DePangher, and A. Andrew, "An Analysis of Non-Uniform Proton Irradiation Damage in Silicon Solar Cells," IEEE Transactions on Nuclear Science, NS-13, Oct., 1966, p. 37.
8. E. Stofel and D. Joslin, "Low Energy Proton Irradiation of Solar Cell Back Contacts," Proc. IEEE Eighth Photovoltaic Spec. Conf., 1970, pp. 209.
9. C. T. Sah, K. A. Yamakawa, and R. Lutwack, "Reduction of Solar Cell Efficiency by Bulk Defects Across the Back-Surface-Field Junction," J. Appl. Phys. 53(4), April, 1982.

Table I. Light I-V Data (AMO, 28° C) of 200 μm Thick Silicon Solar Cells Before and After 1 MeV Proton Irradiation

Irradiation Configuration	BSF	Fluence (p/cm^2)	I_{sc} (mA)	V_{oc} (mV)	P_{max} (mW)	FF
Front Normal	No	0	150.1	539.3	63.23	0.78
		1×10^{12}	89.9	437.6	27.61	0.70
	Yes	0	171.0	608.4	80.78	0.78
		1×10^{12}	95.1	441.1	29.88	0.71
Front Omni	No	0	150.9	538.2	63.15	0.78
		1×10^{12}	104.4	437.9	32.86	0.72
	Yes	0	170.9	607.4	80.48	0.78
		1×10^{12}	113.1	440.4	35.94	0.72
		---	---	---	---	---
Rear Normal	No	0	151.9	537.1	63.28	0.78
		1×10^{12}	150.0	524.0	54.45	0.69
	Yes	0	173.5	605.8	80.99	0.77
		1×10^{12}	158.6	530.7	63.23	0.75
Rear Omni	No	0	152.0	536.8	63.35	0.78
		1×10^{12}	151.4	535.3	62.86	0.78
	Yes	0	171.7	606.4	80.62	0.78
		1×10^{12}	159.4	542.1	67.23	0.77

Table II. Light I-V Data (AM0, 28° C) of 63 μm Thick Silicon Solar Cells Before and After 1 MeV Proton Irradiation

Irradiation Configuration	BSF	Fluence (p/cm^2)	I_{sc} (mA)	V_{oc} (mV)	P_{max} (mW)	FF
Front Normal	No	0	144.5	509.9	56.43	0.77
		1×10^{12}	96.3	434.1	28.43	0.68
	Yes	0	161.2	600.2	72.53	0.77
		1×10^{12}	95.8	434.5	28.59	0.69
Front Omni	No	0	144.9	510.3	56.68	0.77
		1×10^{12}	107.7	435.2	33.60	0.72
	Yes	0	160.2	600.3	72.33	0.75
		1×10^{12}	111.0	436.5	34.97	0.72
		---	---	---	---	---
Rear Normal	No	0	143.6	511.5	56.03	0.76
		1×10^{12}	138.9	493.2	46.13	0.67
	Yes	0	161.7	597.9	72.29	0.76
		1×10^{12}	133.9	485.5	43.97	0.67
Rear Omni	No	0	144.7	511.3	56.09	0.76
		1×10^{12}	142.2	506.5	54.31	0.75
	Yes	0	160.5	601.5	72.41	0.75
		1×10^{12}	137.8	504.2	[illegible]	0.77

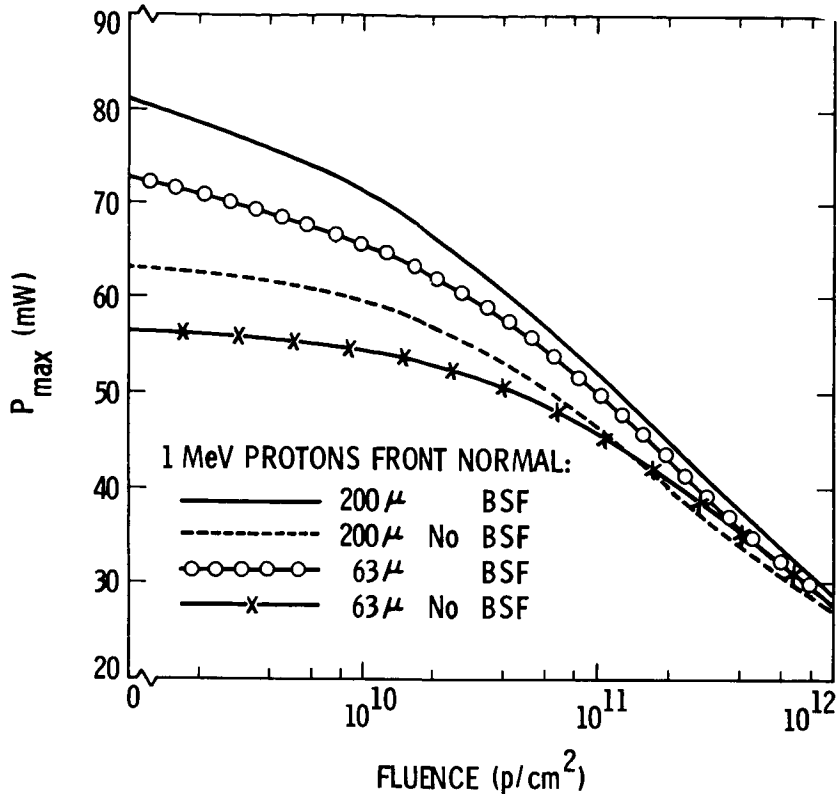

Figure 1. P_{max} of 200 μm and 63 μm BSF and Non-BSF Solar Cells as a Function of Fluence of 1 MeV Front Surface Normal Incident Protons.

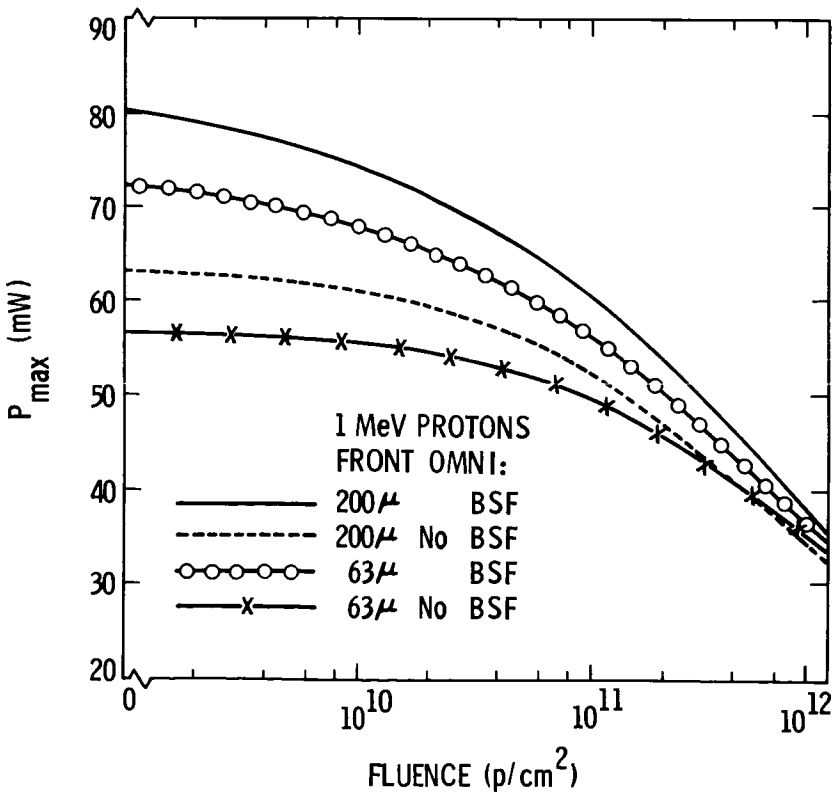

Figure 2. P_{max} of 200 μm and 63 μm BSF and Non-BSF Solar Cells as a Function of Fluence of 1 MeV Front Surface Omnidirectional Incident Protons.

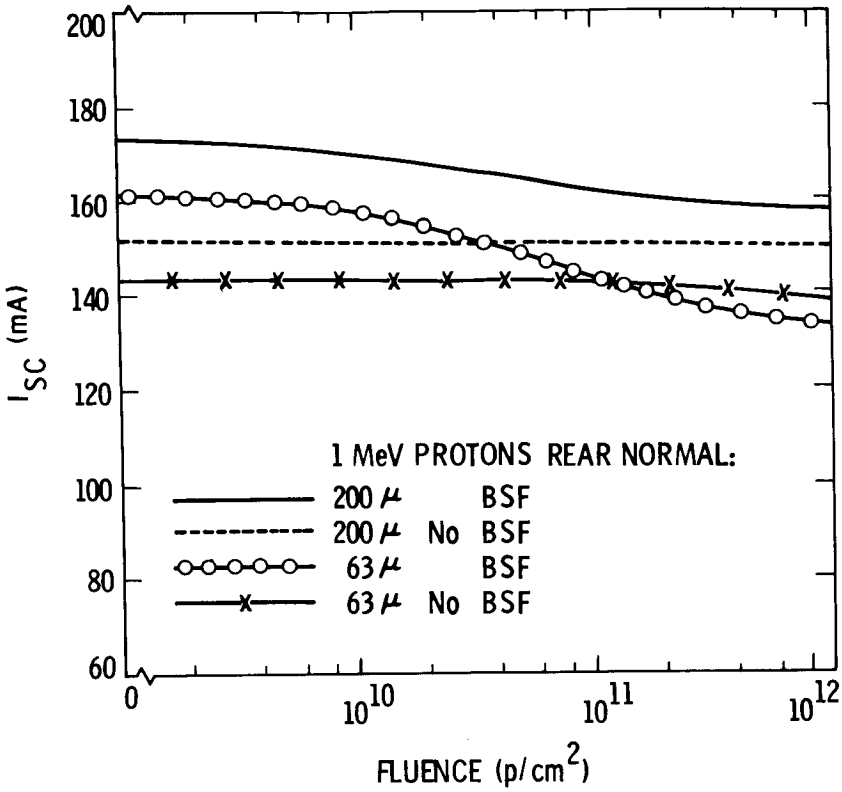

Figure 3. I_{SC} of 200 μm and 63 μm BSF and Non-BSF Solar Cells as a Function of Fluence of 1 MeV Rear Surface Normal Incident Protons.

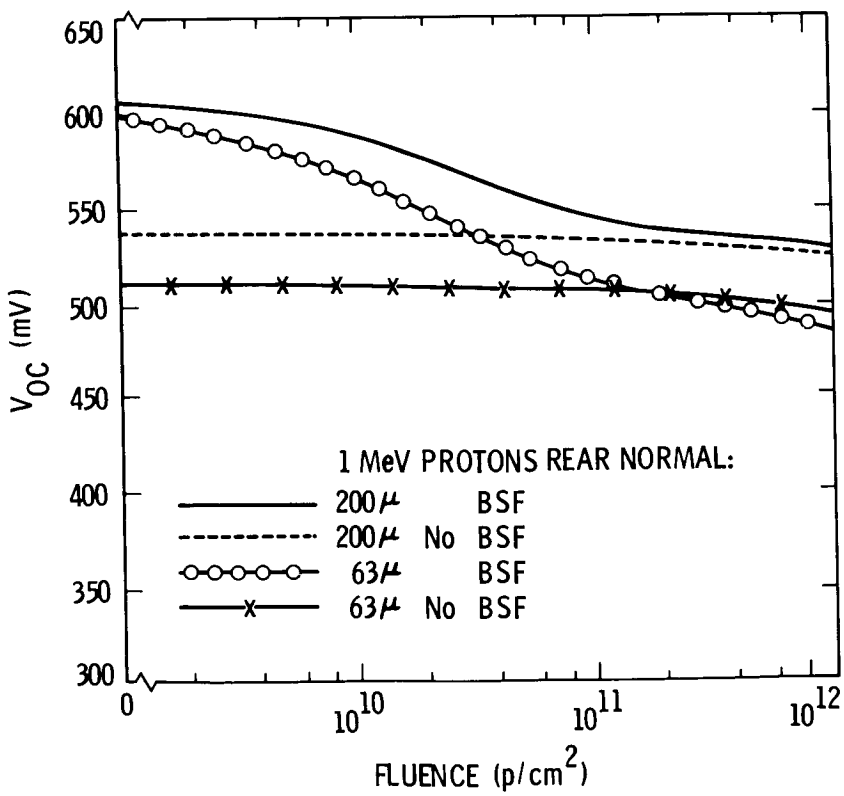

Figure 4. V_{OC} of 200 μm and 63 μm BSF and Non-BSF Solar Cells as a Function of Fluence of 1 MeV Rear Surface Normal Incident Protons.

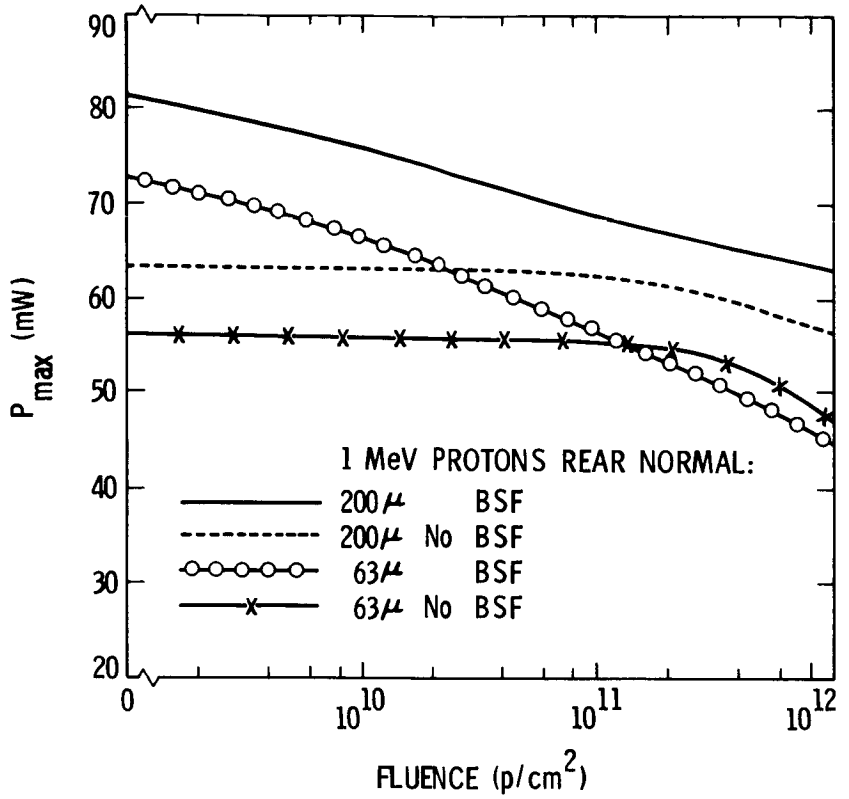

Figure 5. P_{max} of 200 μm and 63 μm BSF and Non-BSF Solar Cells as a Function of Fluence of 1 MeV Rear Surface Normal Incident Protons.

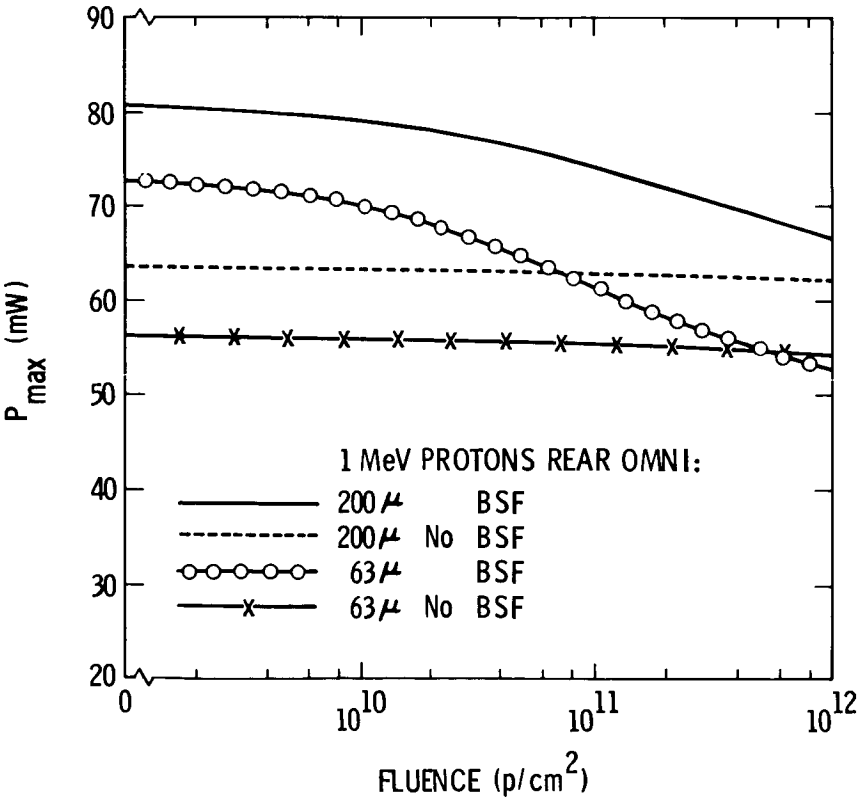

Figure 6. P_{max} of 200 μm and 63 μm BSF and Non-BSF Solar Cells as a Function of Fluence of 1 MeV Rear Surface Omnidirectional Incident Protons.

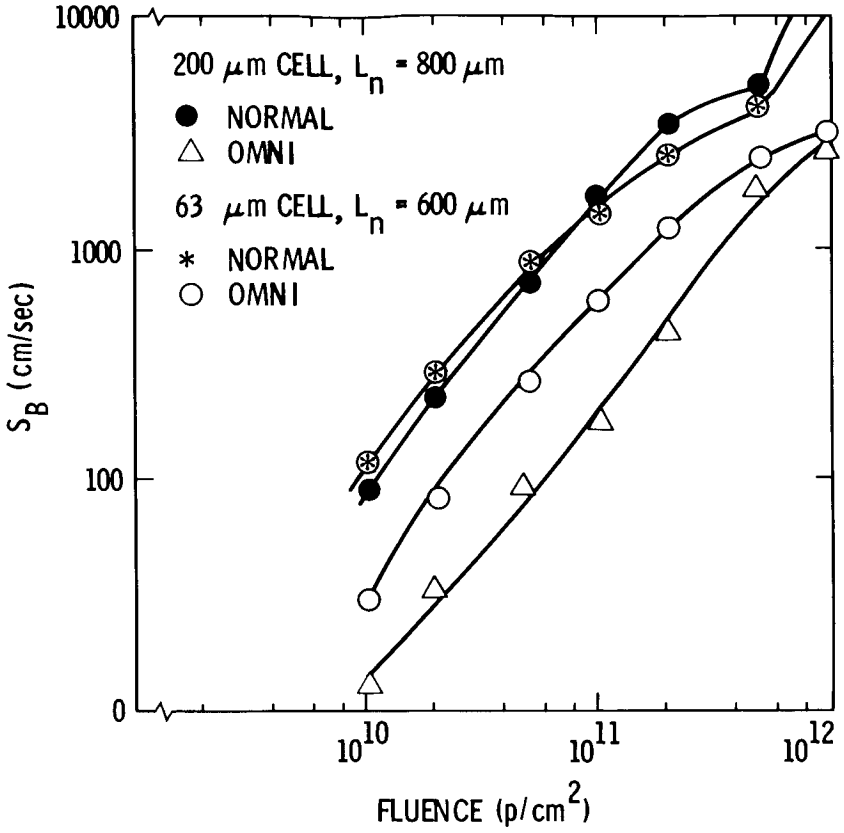

Figure 7. Calculated Back Surface Recombination Velocity of 200 μm and 63 μm Solar Cells as a Function of Fluence of 1 MeV Rear Surface Normal and Omni Incident Protons.